Materials & Design 254 (2025) 114049

Contents lists available at ScienceDirect

Materials & Design

journal homepage: www.elsevier.com/locate/matdes

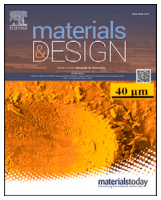

3D concrete printing of topological interlocking blocks

Tom Goertzen [a,d,*], Tobias Neef [b], Philipp Scheffler [b], Domen Macek [c], Viktor Mechtcherine [b], Alice C. Niemeyer [d]

[a] School of Mathematics and Statistics, University of Sydney, Australia
[b] Institute of Construction Materials, TU Dresden, Germany
[c] Institute of Applied Mechanics, RWTH Aachen University, Germany
[d] Chair of Algebra and Representation Theory, RWTH Aachen University, Germany

ARTICLE INFO

Keywords:
Topological interlocking assemblies (TIA)
Sustainable construction
3D concrete printing
Modular design principles

ABSTRACT

In this work the feasibility of combining the concept of *topological interlocking assemblies* (TIA) with 3D concrete printing is investigated. In TIA, blocks are arranged in a manner that, when kinematically constrained by a surrounding frame, all blocks in the entire assembly become immovable solely through the contact between neighbouring blocks, eliminating the need for binding materials. This study aims to investigate whether blocks for a TIA can be produced using 3D concrete printing. For this a method for path planning specially tailored for the manufacturing of TIA blocks, guaranteeing contact between blocks is introduced and three blocks that admit TIA are manufactured. For one block geometry, an assembly with 18 blocks in the form of a slab system is chosen and constructed for further experiments. The structural behaviour of this slab system composed of printed topological interlocking blocks is evaluated by both a finite element method analysis and experimental testing. The findings underscore the feasibility of integrating TIA with 3D concrete printing, highlighting potential applications in sustainable construction.

1. Introduction

In the pursuit of enhancing resource efficiency and minimising environmental impact, the focus has increasingly shifted towards improving the sustainability of materials and structures across various industries, including the construction sector. This drive for sustainability emphasises the need for innovative design approaches and construction principles that prioritize not only the recyclability but also the reusability of materials and components. Traditional construction practices often rely on the use of monolithic components made from high-performance composites tailored for specific applications. These components, while effective in their intended use, present challenges in recycling due to the energy-intensive processes required for their separation and recovery. This dilemma has sparked a crucial question: How can we advance resource efficiency in construction without recycling?

One promising approach to addressing this question is the adoption of modular design principles, where buildings and structures are conceived with reusability in mind from the outset. By transitioning from a traditional, monolithic design paradigm to a modular, component-based approach, it becomes possible to create structures that are not only sustainable but also adaptable. Modular components, designed for easy assembly and disassembly, can be reused in various configurations, significantly reducing waste and energy consumption associated with demolition and recycling. The concept of *topological interlocking assemblies* (TIA) stands out as a particularly innovative solution for modular construction with wide-ranging applications in various fields, see [7,11] for an overview. It involves the design of mortarless structures composed of blocks that interlock kinematically only constrained by a peripheral frame, enabling them to bear structural loads without the need for traditional binding materials. In addition, a peripheral constraint is critical in TIA to prevent disassembly of the blocks, as they fit together purely by geometry rather than friction, mortar or other bonding methods, unlike blocks that rely solely on local bonding performance ([43,48]).

1.1. State-of-the-art

The exploration of topological interlocking assemblies has gained momentum with the study [5], and emerged as a promising strategy for modular design. The innovative approach of TIA is distinguished by its numerous benefits, including the ability to prevent the spread of cracks

* Corresponding author at: School of Mathematics and Statistics, University of Sydney, Australia.
E-mail address: tom.goertzen@sydney.edu.au (T. Goertzen).

https://doi.org/10.1016/j.matdes.2025.114049
Received 16 April 2024; Received in revised form 27 April 2025; Accepted 4 May 2025
Available online 15 May 2025

and maintain structural integrity even with up to 25% of blocks missing [7,10,11,27]. Several design strategies have been explored for topological interlocking assemblies. One approach describes a method for creating structures using convex blocks [21]. Another strategy uses Voronoi domains for block design, see [2,35]. In this work, three blocks are investigated designed by an innovative method inspired by the Dutch artist M.C. Escher, where topological interlocking blocks are obtained by interpolating between two tiles, see [13,14]. Topological interlocking blocks obtained with this method stand out due to their simplicity and versatility, see [12,13].

The application of TIA as a design concept has been investigated by various groups in the architectural context and conceptually proven to be a promising design approach for modular structures, see for instance [16,25,37,39,41,42]. An impressive example is the Armadillo Vault, a large structure with limestone blocks (75 m^2) that was built by cutting limestone to create a large interlocking structure [31].

Manufacturing of topological interlocking blocks with concrete can be approached with conventional methods such as casting with concrete, see [8,18]. Casting of topological interlocking blocks with concrete has been investigated for several block geometries. One type of topological interlocking blocks with curved surfaces that prove promising are *osteomorphic blocks*, resembling bone structures, which are introduced in [6]. In [47] methods for casting osteomorphic blocks together with a mechanical investigation are presented. A similar block design is proposed in [20] and its impact behaviour as cast concrete blocks is experimentally and numerically tested in [18,19]. An overview of the mechanics and manufacturing methods of TIA is further given in [32]. Besides the application of TIA to slab-design, it is also possible to build non-planar TIA. An assembly in the form of a column is presented in [46] and realised as a concrete cast structure in [45].

While the principle of connecting 3D concrete printed elements forms part of many research projects, no published attempt has yet been made to print topological interlocking blocks with concrete or to utilise the effects of TIA for the connection of 3D printed concrete elements. For example, in [4] and [38] a bridge is built by subsequently bracing the 3D printed elements with polymer bearings in between. A similar modular construction approach with 3D printed concrete parts is presented in [26], where a cable-supported 3D printed bridge is built and tested. Another possibility is to insert metallic connecting elements into the layers and overprint them. The modules printed with strain-hardening cement-based composites (SHCC) were later joined together using the connecting elements [17]. The structural hierarchy of corrugated surfaces of topological interlocking blocks is an efficient way in order to enhance the performance of TIA, see [9] and 3D concrete printing of topological interlocking block geometries leads similarly to corrugated surfaces, possibly enhancing the performance. The possibility of 3D concrete printing of blocks with a locking mechanism is discussed in several works [8,40] and experiments on the bonding performance of 3D concrete printed surfaces with vertical geometry have been investigated in [43,48]. However, printing TIA blocks using 3D concrete printing presents unique challenges: many TIA blocks feature steeply inclined surfaces, may include pointed corners or both inward- and outward-sloping walls. Achieving the precision required for these intricate geometries is particularly demanding, and there is neither a report in the literature on 3D-concrete-printed topological interlocking blocks nor on TIA consisting of such blocks.

1.2. Hypothesis

In this work, we investigate the hypothesis that *TIA can be manufactured using 3D concrete printing techniques*. There are several key challenges that need to be addressed in order to verify this hypothesis: choosing suitable block geometries, developing a method for path-planning, manufacturing blocks with sloped surfaces using 3D concrete printing with adequate precision, predicting the mechanical behaviour (e.g. performance) of the chosen assembly by utilising numerical methods, such as FEM simulation, and finally experimental testing and applications of the resulting structures.

From a theoretical point of view, the interlocking mechanism within a TIA only depends on the contact regions of the boundaries of two neighbouring blocks, see [15,44]. Thus for the interlocking property, the contact surface of the blocks plays a key role and one can also consider hollow topological interlocking blocks such that the surface can be approximated by a 3D printing path. In [24], the design and analysis of beam-like structures with hollow tetrahedral elements are investigated. While using hollow blocks leads to significant material saving, it has been demonstrated that the cellularity of the blocks, e.g., wall thickness of hollow blocks, has a strong influence on the overall performance of the TIA, see [22] in the case of 3D printed polymer blocks.

We verify the hypothesis by choosing three simple geometries in Section 2 that are obtained from the methods presented in [13] and are suitable for the path-planning method custom-tailored for topological interlocking blocks developed in Section 3. One of the three geometries is selected for the construction of a TIA slab system consisting of 18 blocks, providing a first approach to the question of the feasibility of combining TIA with 3D concrete printing. In Section 4, numerical simulations depict the behaviour of this system under load. In Section 5, materials and methods for printing the blocks are presented. Moreover, the assembly of the chosen TIA together with its frame is described. In Section 6, the load test of the TIA consisting of 18 blocks using a 3D photogrammetric measurement system is described and analysed. Finally, in Section 7 we draw the conclusion that topological interlocking blocks can be successfully manufactured using 3D concrete printing and employed in large-scale structures.

2. Modelling and construction of blocks

This work focuses on the construction of blocks based on the methods presented in [13]. Here, the main idea is to interpolate between tiles of two tessellations, admitting the same symmetry, using an Escher-like approach. For example, in Fig. 1 the block is obtained by interpolating between a square and a rectangle placed in two parallel planes, i.e. the square “grows out of the plane” into a rectangle, see [13]. The underlying symmetries correspond to wallpaper symmetries, which are also known as planar crystallographic groups, mapping one tile of the given tessellation to another. In this work, blocks are considered which are constructed from tiles of one of the wallpaper groups p1, p4 or p3 (using the Hermann–Mauguin notation [3]). Blocks created with this method are chosen for their suitability for 3D printing applications as they possess a geometry which can be described by relatively few triangles per block and the printing path can be computed as detailed in Section 3. Moreover, the surface of the blocks can be approximated by considering layers of the block whose boundary can be obtained by a piecewise-linear printing path. For this, the top and bottom faces are omitted, leading naturally to hollow interlocking blocks with vertical as well as inclined faces.

For testing the 3D printing process, three blocks are chosen as candidates, named *Versatile Block*, *RhomBlock* and *3-Diamond Block*, which are generated using the methods presented in [13]. For 3D-printing purposes, we consider hollow block geometries since they can be best approximated using a printing path. For better visualization, the block geometry and possible TIA are shown in Figs. 1–3, with the bottom and top faces closed. The frame consists of the outermost blocks, marked in white. The resulting 3D-concrete printed blocks are shown in Fig. 12. Both the *Versatile Block* and the *RhomBlock* also possess a versatility property that makes it possible to create assemblies with copies of them in several ways, see [14]. These specific blocks have been chosen, as together their geometries present different challenges for the 3D-printing process: the Versatile Block has steep inclined faces, the RhomBlock is very pointed and the 3-Diamond Block has several inward- and outward-inclined faces.

Fig. 1. The design of the Versatile Block (a, b) encapsulates the symmetries of various crystallographic groups and can be obtained by interpolating between a square and a rectangle, see [13]. It is part of a larger family of versatile blocks with the distinguished property of having a large contact area to its neighbouring blocks in a TIA compared to its overall surface area, see [14]. Moreover, different planar assemblies of the Versatile Block can be used for various applications as the load distribution depends strongly on its various arrangements, see [1,12]. The block can be assembled in a right-angled configuration, making it ideally suited for the use in conventional building constructions. It can be arranged into a TIA (c) with outer frame (in white) being fixed.

Fig. 2. The RhomBlock can be viewed as a hexagonal counterpart of the Versatile Block, as it allows many distinct planar assemblies, which can be also characterised by generalised Truchet tiles, see [14]. The bottom tile is given by a lozenge tile, i.e. a rhomb consisting of two equilateral triangles, and the top tile by a hexagon. The *RhomBlock* (a, b) is obtained by interpolating between the bottom (lozenge) and top tile (hexagon). The contact to neighbouring blocks of the blue middle block is indicated by the white outer blocks. It can be, for instance, arranged into a TIA (c) with outer frame (in white) being fixed. The assembly is obtained by the actions of the wallpaper group p3: rotating copies of the block by 120 degrees and shifting three such copies by hexagonal translations.

Fig. 3. The *3-Diamond Block* (a, b), see [13], is characterised by the large contact area with neighbouring blocks. This leads to a large degree of interlocking since one block is supported by three blocks from below while simultaneously supporting three blocks itself, whereas for the RhomBlock and Versatile Block only two neighbouring blocks are being supportive and supported. The contact to neighbouring blocks of the blue middle block is indicated by the white outer blocks. Using translations only, it can be arranged into a TIA (c) with outer frame (in white) being fixed.

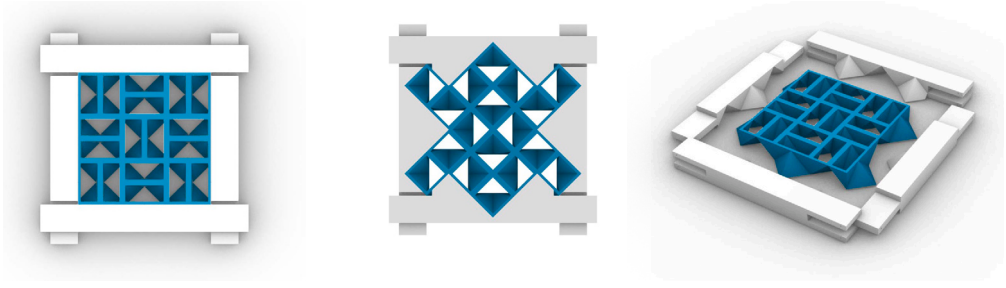

Fig. 4. Model of the chosen assembly, together with frame components: (a) top view, (b) bottom view (c) exploded perspective view displaying the frame composed of four parts.

For further analysis and testing, a special assembly using Versatile Blocks is chosen, see also Section 5 for further reasons. To ensure interlocking within the assembly, it suffices to restrain the outer blocks from moving using a peripheral constraint, see Fig. 1, due to the property of being a TIA. Instead, one can also design custom-shaped components for the frame that adapt to the geometry of the underlying blocks. The entire model consisting of 18 hollow Versatile Blocks together with the frame (in white) is shown in Fig. 4. Here, we consider hollow blocks because they can be naturally approximated using printing paths, allowing for material savings while preserving the interlocking property, see Section 3. A moment resisting frame is given by four parts, where the opposite two parts are equal and ensure no displacement of the blocks

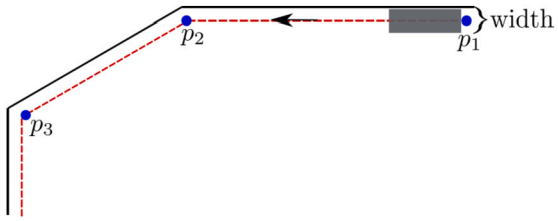

Fig. 5. Computing the print path (red dashed line) with offset $width/2$ from the original boundary surface of the geometry (black line) corresponds to computing points $p_1, p_2, p_3, \ldots$ and a piecewise-linear path following these points.

in all directions. Holes in the frame allow adding steel reinforcement using threaded steel rods to put tension onto the assembly. The shape of the frame is chosen to be moment-resisting, by its contact to other frame parts.

3. Path-planning and software workflow

In this section, a path-finding method for the 3D-concrete printing of topological interlocking blocks is introduced. This method addresses several challenges to ensure the generation of a piecewise-linear printing path suitable for manufacturing 3D-concrete printed blocks in a topological interlocking assembly. The resulting path has two essential properties: continuity, ensuring an uninterrupted printing process without pauses, and no crossings, preventing excess material deposition in certain regions.

In 3D printing applications, one typically begins with a predefined geometry, such as a triangulated mesh in an STL file, with the goal of producing a printed geometry that closely replicates the original shape or possesses similar geometric properties. More precisely, the initial shape is approximated using a piecewise-linear printing path. The printing path is given as a list of points $P = [p_1, \ldots, p_n]$, also known as *point cloud*, and the path is obtained by a piecewise-linear interpolation from point p_i to point p_{i+1} for $i = 1, \ldots, n-1$. In Fig. 5, a printing path for a given width, such that the boundary of the resulting geometry is as-close-as-possible to the initial one, is shown.

The geometry of the given blocks, presented in the previous section, allows a straightforward approach for finding a 3D-path. There are several key aspects that have to be considered:

1. What are the parameters of the path (width and height)?
2. How can the interlocking property of the manufactured blocks be retained?
3. How can one ensure that the 3D-printed geometry is as close as possible to the initial given shape?

The scale for the 3D concrete printer used in this work differs significantly from conventional polymer printers leading to several challenges that need to be addressed in the computation of the printing path. The pumped concrete is extruded through a round nozzle with a diameter of 19 mm, producing layers with a width of 25 mm and a height of 5 mm. This layer geometry is determined by the balance between the extrusion flow rate and the concrete's deposition speed. Moreover, the printer uses a constant pump that does not allow stopping at certain points and resuming printing at another point, leading to the necessity of computing a continuous printing path.

The interlocking property and the 3D printing technique both share the focus on the boundary as a material design concept. For interlocking purposes, the contact surfaces of two neighbouring blocks are essential, which has to be part of the path finding algorithm. For the development of the path, it is assumed that the 3D concrete printer requires a constant flow rate and a constant nozzle speed to produce a uniform width of the deposited concrete strand.

This work restricts to the case, where both the bottom and top surface of the given geometry are planar surfaces which are omitted, and only the outer perimeter of the given geometry is printed which can be given as a continuous printing path. In 3D-printing software for commercial printers this printing mode is usually referred to as *vase mode*.

To ensure smooth transitions between layers, the connection point where one layer ends and the next layer begins must be carefully planned. Instead of directly starting the next layer at the exact endpoint of the previous one, the printing path is designed to place the starting and ending points of consecutive layers slightly apart. This separation helps to avoid abrupt changes in nozzle direction, which can occur if the nozzle loops back sharply. By planning the path this way, the nozzle movement remains smooth and consistent, minimising turning points and maintaining a steady flow rate.

Due to the width of the printing path and the resulting offset of $width/2$ from the original boundary of the geometry, it can happen that for short edges and steep angles the computed path has a self-crossing, see Fig. 6a. Compared to polymer printers, the control of the material flow is hard to achieve. As previously mentioned, the flow rate of a concrete 3D-printer is constant to avoid blockage in the hose, which can lead to an over extrusion of concrete at the crossing point. In this case, one needs to modify the path: first compute all crossings and then disregard certain parts of the initial path, see Fig. 6b.

In Fig. 7, two computed printing paths for the Versatile Block are shown. The path in Fig. 7a contains crossings (see red circle) with a closer view given in Fig. 7c. After determining these crossings, the path-finding method alters the printing path at these regions, as shown in Fig. 6, leading to a new path without crossings, see Fig. 7b.

Software workflow The original block geometries are given as triangulated surfaces and can, for instance, be realised as STL-files. Next,

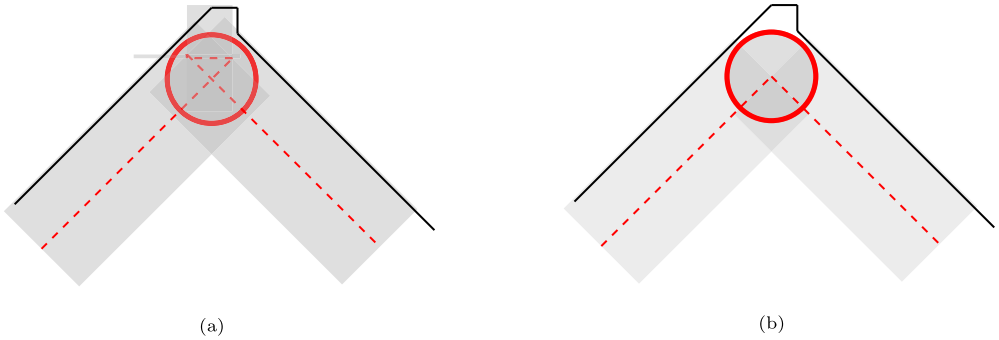

Fig. 6. (a) Illustration of a naive path computation for a 3D printing boundary with an initial path (red dashed line) approximating the original boundary (black line) containing self-crossings due to the narrow width of the boundary relative to the printing path width (grey), resulting in localised material buildup as shown by the varying grey intensities. (b) A corrected path, where self-crossing segments have been omitted, achieves a crossing-free path to prevent material over-extrusion around crossing parts.

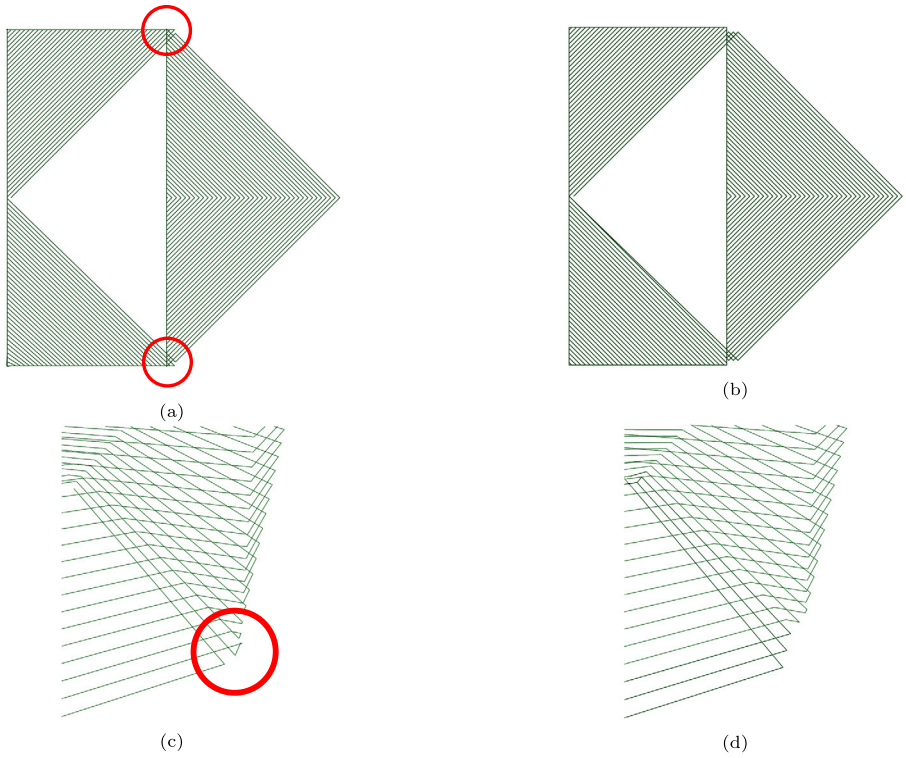

Fig. 7. Example of paths with and without crossings for the Versatile Block: (a) top-view and (c) side-view of path with crossings and (b) top-view and (d) side-view of the path without crossings.

one can compute all edges connecting the bottom and top surface of a given block and compute a continuous printing path that travels along the boundary for each printing layer using the method described above. The resulting path is given as a point cloud and imported into the CAD software Rhinoceros 3D to obtain a Kuka language generation, which can be used to control the robot arm that determines the position of the printing nozzle.

4. Numerical analysis of the chosen assembly

In the following, the topological interlocking assembly consisting of 18 Versatile Blocks, as shown in Fig. 4, is numerically analysed to gain insights into and better understand the mechanical behaviour of the system. Here, a scenario of applying load to the two middle blocks as conducted during the mechanical test, see Section 6, stands in the foreground. For numerical simulations of TIA consisting of 64 Versatile Blocks, where an equal load is put onto all blocks, see [12]. The mechanical analysis was performed using the commercial finite-element software Abaqus/CAE 2022.HF1.

To investigate the static response of the periodic arrangement of the Versatile Block, quasi-static analyses were performed. The geometry of the Versatile Block is non-convex and intricate, leading to highly complex contact conditions between the blocks. While the deformations of the blocks were assumed to be small (following linear strain theory), the blocks were still allowed to undergo finite rotations. Due to the high complexity of the mechanical system, explicit dynamics FEM algorithm (ABAQUS/EXPLICIT) was used to improve the simulation efficiency. The simulation was performed without mass scaling to ensure that the dynamics of the system was accurately represented throughout the analysis.

The blocks were modelled as isotropic and linear elastic material, made of concrete, with properties listed in Table 1. These values correspond to the material used in the experiment. For simplicity in simulation and to provide a first estimation of the mechanical behaviour of the assembly, it was assumed that the blocks have perfectly smooth surfaces. However, this does not fully reflect real-world conditions. Frictional contact between all blocks was defined using an exponential pressure-overclosure relationship. According to Abaqus definitions, the following parameters were specified: a clearance between the bodies, $c_0 = 0.02\,\mathrm{cm}$ (measured in the contact normal direction), a contact pressure at zero clearance, $p_{c_0} = 0.5\,\mathrm{N\,cm^{-2}}$, and a friction coefficient of 0.55 for dry contact between concrete surfaces. Each block was meshed individually using 4-node tetrahedral elements. For a detailed explanation of the simulation setup, refer to [12].

Table 1
Simulation parameters.

Parameter	Value	Description
ρ [kg cm^{-3}]	2400×10^{-8}	Density
E [N cm^{-2}]	33×10^{5}	Young's modulus
ν [–]	0.2	Poisson's ratio
μ [–]	0.55	friction coefficient
α [–]	2.0	Mass proportional damping
β [–]	$1.0 \cdot 10^{-8}$	Stiffness proportional damping

Displacement boundary conditions were applied by fully constraining the bounding frame in space (see Fig. 8). A transverse pressure of $p_0 = 15.9272\,\mathrm{N\,cm^{-2}}$ was applied to the top surfaces of the two central blocks, as illustrated in Fig. 8. This pressure corresponds to the force (8.76 kN) applied during the experiment, see Section 6. Quasi-static loading conditions were maintained throughout the analysis. To account for damping, both a term related to the volumetric strain rate and a term proportional to the square of the volumetric strain rate were included. Material damping was used to suppress both low-frequency (mass-dependent) and high-frequency (stiffness-dependent) responses (see Table 1).

Contact forces We begin by examining the contact pressure between the blocks and between the assembly and the frame. The contact pressure ($p_0 = F/A$) indirectly reflects the distribution of forces within the TIA (between blocks) and directly impacts the stress fields within the blocks. The results are presented in Fig. 9. According to the friction law, the tangential forces are proportional to the normal forces.

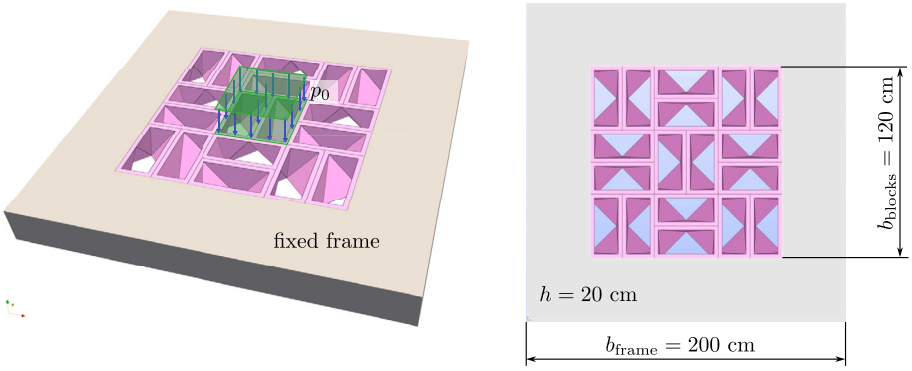

Fig. 8. Schematic representation of the boundary conditions applied to the TIA. The frame is fixed in space, constraining the $p4$ arrangement of Versatile Blocks. A pressure p_0 is applied to the top surface of the two central blocks.

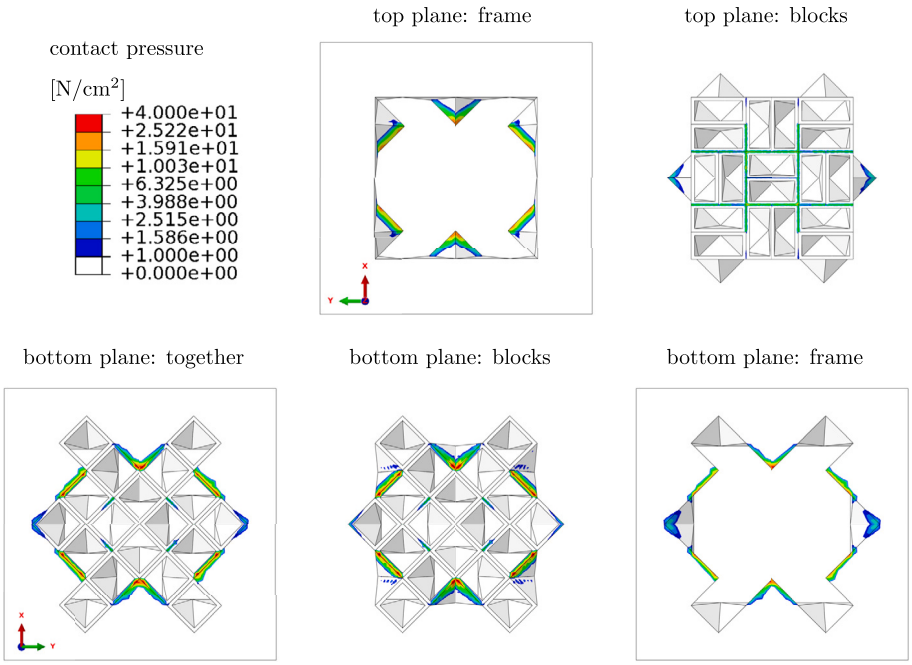

Fig. 9. Contact pressure (FEM simulation) between the blocks in the TIA and the blocks and the frame. The first row represents the top plane, and the second row represents the bottom plane. Due to the symmetry of the Versatile Block and the assemblies, symmetry can also be observed in the contact pressure distribution.

In the top plane ($z = 20\,\text{cm}$) of the assembly, contact pressure is confined to the assembly itself, with the highest values concentrated around the two central blocks. The pressure at the interface between the assembly and the frame edges is nearly zero. Notably, the tips of the middle-left and middle-right blocks exhibit higher contact pressure, indicating that they "lock" into the frame, restricting rotation. On the frame, the upper side of the tips bears the highest stress, effectively "holding" the assembly in place. These areas serve as key points for force transfer from the assembly to the frame.

In the bottom plane ($z = 0.0\,\text{cm}$), the highest contact pressure is primarily observed at the interface between the frame edges and the assembly. Interestingly, only alternate block edges adjacent to the frame experience significant stress, indicating that not all block edges along the frame contribute to force transfer. Additionally, the four corner blocks of the assembly experience almost no contact pressure.

We note that the distribution of contact forces within the assembly resembles the load transfer paths identified in [22–24] and described in detail in [36].

Distribution of stresses Fig. 10 shows the distribution of the maximum and minimum principal stresses within the assembly. The maximum principal stress, representing the most tensile stress, is an effective indicator for predicting cracking, given concrete's very low tensile strength. In contrast, the minimum principal stress — the most compressive — serves as a valuable measure, alongside contact forces, for visualizing load transfer within the TIA. The stress distributions are highly complex, largely due to the non-convex geometry of the blocks. Particularly noteworthy is the transfer of stress from the top plane, where the load is applied, to the bottom plane.

Due to the $p4$ symmetry of the assembly, only one-quarter of it (highlighted by the dashed pink square) needs to be analysed. The distribution of the maximum principal stress on the bottom plane ($z = 0$ cm) indicates that the critical points of the assembly are located at the bottom corners of the block tip (highlighted with a red circle in Fig. 10a). At these points, the stress reaches approximately $590\,\text{N}\,\text{cm}^{-2}$ (equivalent to 5.9 MPa). The stresses at these critical locations can be compared to the concrete's cracking tensile strength to assess the performance of the assembly. This area of the block is also a prime candidate for fibre reinforcement. On the top plane, the lowest minimum principal stresses are concentrated at the interfaces where the two central blocks meet the adjacent left and right blocks (highlighted with a blue circle in Fig. 10b) and reach approximately $-850\,\text{N}\,\text{cm}^{-2}$ (equivalent to -8.5 MPa).

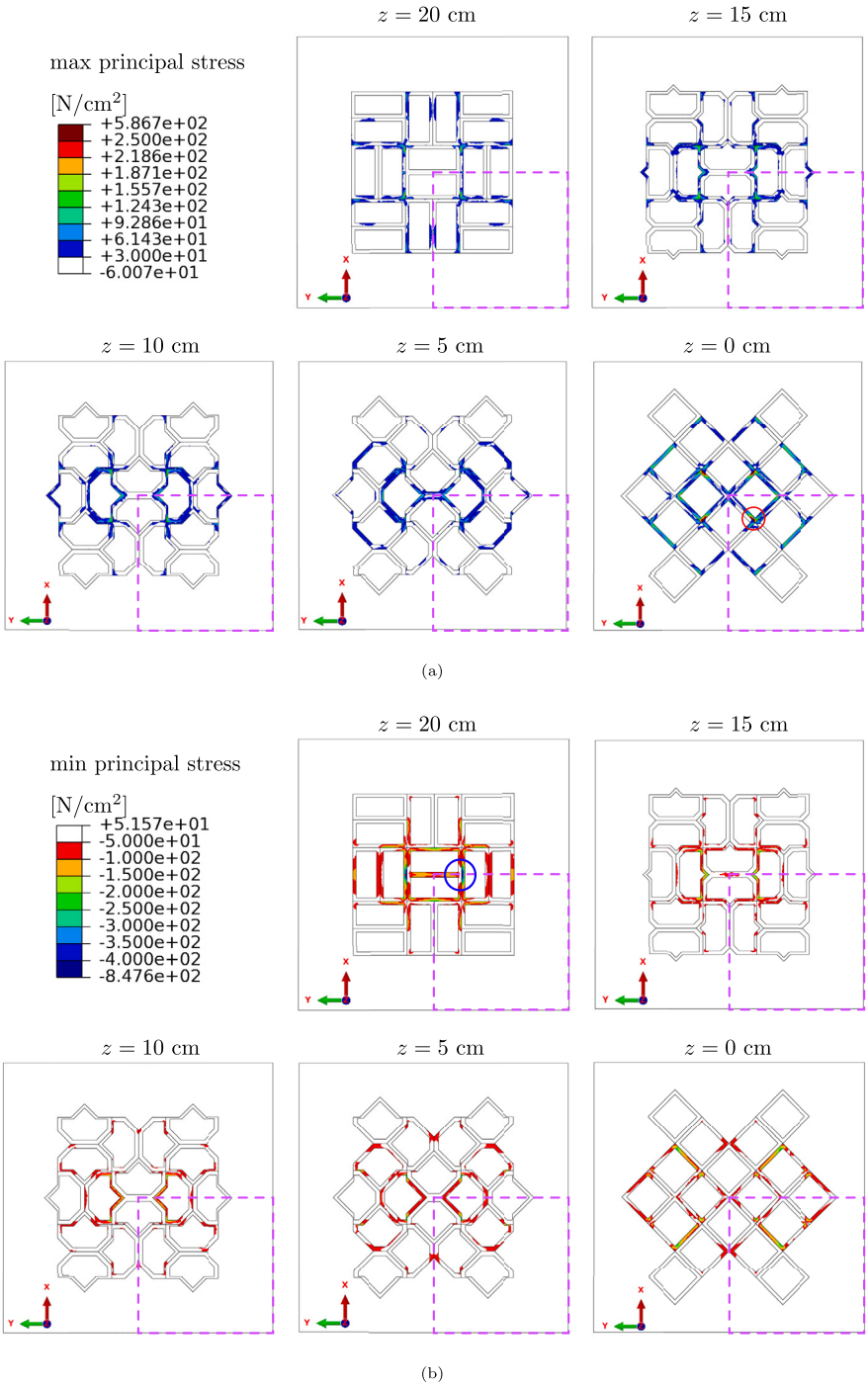

Fig. 10. Principal stress distributions (maximum and minimum) in five planes of the TIA ($z = 0$ cm, $z = 5$ cm, $z = 10$ cm, $z = 15$ cm and $z = 20$ cm). Due to the symmetry of the Versatile Block and the assembly, symmetry (dashed pink square) can also be observed in the stress distribution. The red and blue circles highlight the critical points in the TIA.

As a side note, we would like to mention that failure of a TIA may occur not only due to wall cracking but also as a result of a global instability mode.

Deformed state and maximum deflection at a given load Fig. 11 shows the displacement fields u_z in z-direction of the TIA. The displacement u_z is shown because the deformation in z-direction is most dominant due to the loading direction.

The deformation patterns of the interlocking assemblies align well with those observed in the experiments (Fig. 18). The results indicate a difference in displacement distribution between the top and bottom planes of the TIA, which is attributed to the local rotation of the block tips.

Within the assembly, deformation is uniformly distributed, leading to the maximum deflection occurring at the centre where the external load is applied. This behaviour is consistent with expectations (see [12]). On the top plane, the maximum displacement is approximately 3.3 mm, while on the bottom plane, it increases to around 3.7 mm due to the local rotation of the block tips.

When comparing these results with experimental observations (Fig. 17), the simulation shows good agreement with reality. However, it is important to note that the maximum displacement observed in the

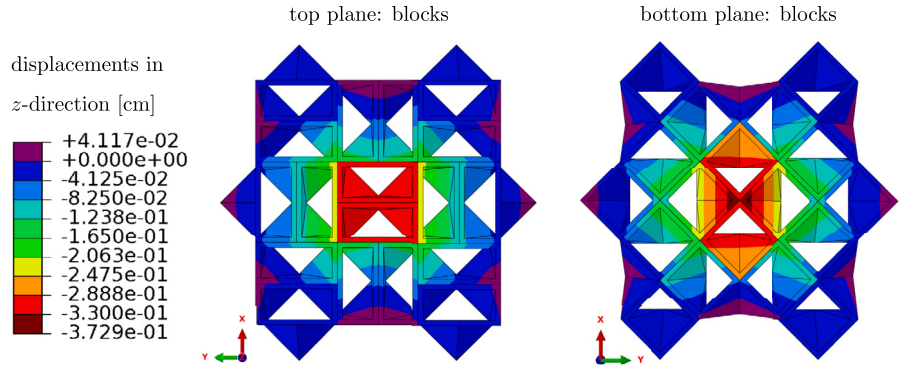

Fig. 11. Displacements in z-direction. This figure shows displacement fields in z-direction on the top ($z = 20$ cm) and bottom ($z = 0$ cm) plane of the three TIA. The maximum deflection occurs at the center of the assembly, with the highest displacement observed on the bottom plane, reaching 0.3729 cm.

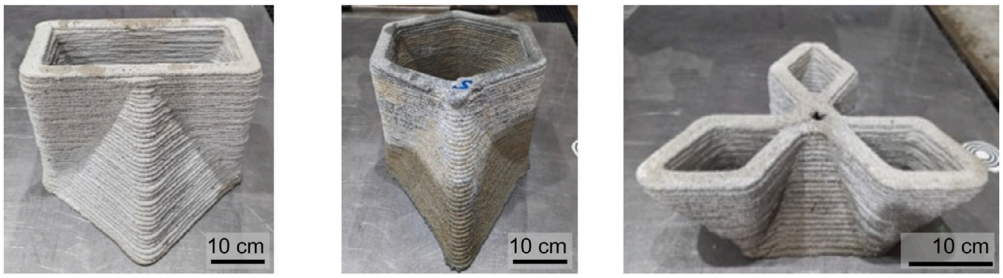

(a) (b) (c)

Fig. 12. Resulting 3D concrete printed blocks of (a) Versatile Block, (b) RhomBlock and (c) 3-Diamond Block.

experiments (blue curve in Fig. 17) is approximately 0.5 mm higher, which can be attributed to the influence of the dead load.

5. Materials and methods

In Section 3 the theoretical foundation on which the generation of printed geometries is based is explained. All of the three presented topological interlocking blocks in the Section 2 were 3D concrete printed. However, only one was selected for mass production and tested in an assembly due to its superior suitability for practical implementation, as outlined in the selection criteria below. The following sections explain the materials used for the printing process and the experimental conditions in the test environment.

5.1. The selection criteria for the block-production and further testing

To ensure smooth production of multiple topological interlocking blocks with consistent geometry, the suitability for mass production of the presented topological interlocking blocks is assessed.

The computed printing paths for the 3-Diamond Block often cross which leads to artefacts during printing. The contact area of the Versatile Blocks to its neighbouring blocks in an assembly is larger compared to the RhomBlock (its hexagonal counter-part). Moreover, since the Versatile Block (Fig. 1), admits a topological interlocking assembly in a rectangular grid compared to the RhomBlock and Diamond Block (Fig. 12) and due to its versatile and simple nature, it was chosen for large-scale production and further experiments. The measurements of the Versatile Block are given as follows: the top rectangle has an area of 20×40 cm^2, the height of the block is 20 cm and the bottom square has an area of 28.28×28.28 cm^2. Note that these areas are approximately equal by design.

5.2. Fine grained concrete for printing

Fine grained 3D printable concrete is used and described in various works, see [29,30]. The selected particle size distribution is important for pump and build-ability and influences the choice of raw materials. In order to ensure a good pumpability and workability, Elkem's Microsilica Powder 971 (MS) was chosen as finest material. To bridge the gap between the Microsilica Powder, the next larger fraction consists of Dyckerhoff's ultra-fine ground cement Microdur R-X, with 95% of its particles smaller than 6 µm and the ordinary cement CEM I 42.5 R from Holcim.

Regarding the sand component, it comprises BCS 413 quartz fine sand and locally available sands with a grain size ranging from 0 to 1 mm and from 0 to 2 mm, respectively these well-developed grain size distribution is essential for achieving the desired composition and properties of the concrete mixture.

Once all the fractions are dry mixed for 1 minute, water and superplasticiser are added and mixed for 3 minutes. To extend the workability, a retarder is added and mixed for 1 minute. This ensures a printing window of 2 h. A good consistency for additive manufacturing with the described setup has a flow spread on the Haegermann table [24] measuring 17.5 cm after compaction strokes. The mixture of the 3DPC is outlined in Table 2. The concrete achieved, in a 3-point-bending-test, a strength of 6.1 [0.6] N/mm ^{2} and a compressive strength of 88.0 [7.5] N/mm ^{2} measured on moulded mortar prisms 1600x40x40 mm ^{3}.

5.3. Printing setup

The manipulator system, see Fig. 13, used to print the topological interlocking blocks, consists of several components, which are a mortar pump for a continuous concrete delivery with a maximum grain-size of 2 mm. The concrete is pumped through a 15-meter-long mortar hose with a nominal diameter DN25, extending to the end of the robot arm.

The pumped concrete is extruded through a round nozzle with a diameter of 19 mm, shaping the material into layers with a width of 25 mm and a height of 5 mm. This shaping results from the interaction between the extrusion flow rate and the deposition speed of the concrete, which were verified during the setup and maintained constant throughout the printing.

Table 2
Composition of a fine concrete for 3D printing [kg/m^3].

OPC I	OPC II	MS	Fine sand	Sand	Sand	Water	Superplasticizer	W/B
d95 < 6 µm	d95 < 9 µm	d95 < 44 µm	0.06/0.2	0/1	0/2			
395	335	14	230	370	795	279	17	0.42

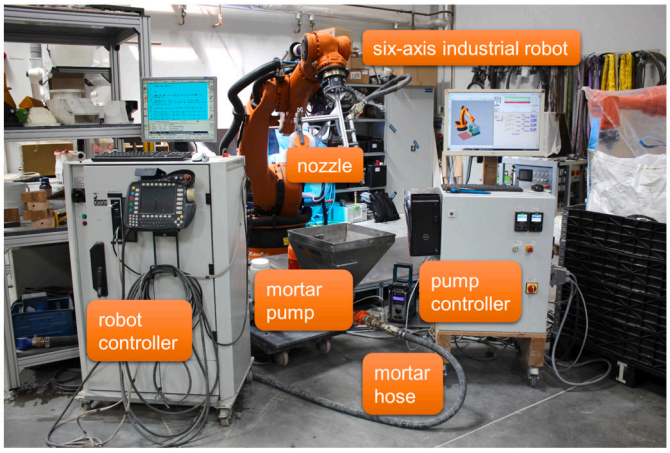

Fig. 13. The manipulator system consists of a motar pump, motar hose, robot, nozzle and control cabinet for the pump and robot.

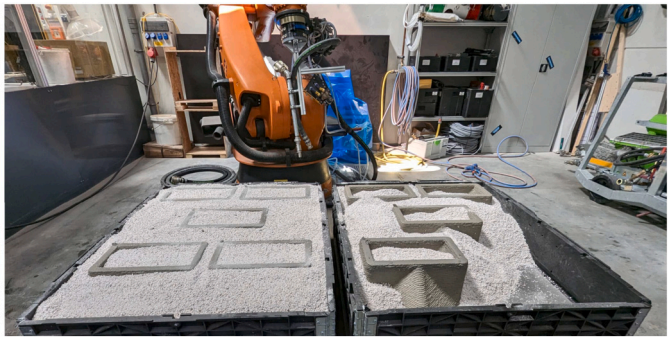

Fig. 14. Print setup with robot, nozzle in the background and print base in front with 9 pre-printed topological interlocking blocks.

A six-axis industrial robot of the KR 240-2 2000 type, manufactured by KUKA, was used for the deposition of the concrete strands. A control cabinet, the KRC2 controller, reads the previously generated printing path and a second control cabinet is controlling the mortar pump and other components. Two pallets made of aluminium profiles measuring 100x1200 mm^2 are used as the printing base and are aligned in a horizontal position.

5.4. Printing of topological interlocking blocks

The production of topological interlocking blocks was conducted in two batches, with each batch comprising nine blocks. This approach was adopted due to the constraints in printing space on the two pallets. If more pallets were available, continuous printing of topological interlocking blocks would not be a problem. Printing was carried out with a round nozzle with a diameter of 19 mm at a printing speed of 10 cm/s. Printing the first 9 blocks took less than 2 hours, see Fig. 14. However, this time can be further reduced by repeating the process and establishing a routine.

During production, the blocks were filled step by step from all sides with fill material to support the fresh concrete and prevent any deformation like buckling or collision. This is necessary due to the inclined surfaces of the block geometry to ensure that the blocks can be assembled into a TIA. A high degree of accuracy was essential for the success of the project. The filler is a commercially available insulating from perlite with a density of 0.9 t/m^3, as used in the construction of wooden ceilings. Furthermore the surrounding fill acts as a foil preventing the concrete from drying out and hinders the flow of hydration heat. This leads to heating in the fill of up to 50 °C and improves the properties cured concrete. Shortly after the printing process, the blocks and the fill material were wetted. After 24 hours the fill is removed and the blocks were stored for 28 days in a normal climate condition at a temperature of 21 °C and a humidity of 70%. The simplest and quickest measurement method for determining the geometric accuracy is to measure the mass, as this correlates with the accuracy. The average mass of the blocks from batch 1 was 16.3 kg, with a standard deviation of 5%, corresponding to a volume of approx. 13 litres. For batch 2, the average mass was 15.9 kg with a standard deviation of 3.8%. The mass is a measure of the accuracy with which a block was printed, so this could be increased in the second batch.

5.5. Production of the frame

In TIA, blocks are arranged in a manner that, when kinematically constrained by a surrounding frame, all blocks in the entire assembly become immovable solely through the contact between neighbouring blocks, eliminating the need for binding materials. To create a frame, the topological interlocking blocks were placed in the plane and assembled in the favoured arrangement, see [12] for a comparison of different assemblies with the Versatile Block. 18 Versatile Blocks are arranged within a slab measuring 130 cm × 130 cm in area and 20 cm in height. Although the frame could have been 3D printed, a cast version was chosen instead due to the limited workspace of the robot. The frame is specifically tailored to this assembly and consists of four cast components. These parts are designed to interlock and can be secured together using threaded rods (see Fig. 4). Care was taken to ensure that the topological interlocking blocks have the best possible contact with each other and interlock firmly. This ensures that the normal force is transmitted equally over all blocks. The outer topological interlocking blocks form one formwork wall of the frame, while the other formwork walls were constructed using OSB (oriented strand board), see Fig. 15a. In order to be able to demount the frame again later and only test the interlocking property, a closed separating foil was placed on the blocks and formwork panels. A sufficiently dimensioned opening is realised using XPS and ensured that the frame could be screwed together later. Plastic tubes formed the empty conduits for the threaded rods M18, which were later used to screw the frame parts together, see Fig. 15b. The heavy, robust frame looks oversized. However, as the notches of the blocks reach very deep into the frame, it is only 5 cm thick at its thinnest point. High frame rigidity is important in order to achieve surface contact with all the blocks. A self-compacting and high-strength concrete C3-B2-HF-2-145-5 was used [33] to cast the frame. The composition and the most important properties are summarised in Table 3.

6. Load test of the composite ceiling

6.1. Test setup

Firstly, the topological interlocking blocks were placed as closely together as possible and the nuts on the threaded rod were tightened gradually and evenly. By slowly closing the frame, a horizontal force is applied and the individual blocks could be optimally arranged. This

Table 3
Composition of the self-compacting concrete C3-B2-HF-2-155-5 [kg/m^3].

CEM VI/S –LL 52.5 N BMK D-1	Quartz Sand 0.06/0.2	Sand 0/2	Grit 2/5	Superplasticizer Liesen 877	Water	W/B	Compressive Strength [MPa]
621	250	530	837	17	155	0.25	112

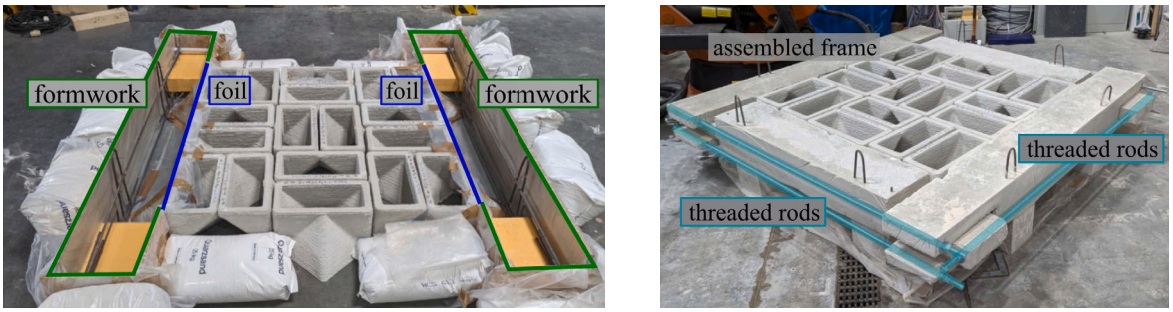

Fig. 15. (a) Fabrication of the frame around the assembled topological interlocking blocks. Blocks and frame are separated by a foil, the green line shows the formwork. (b) The assembled frame is held together by threaded rods and placed on concrete blocks for testing.

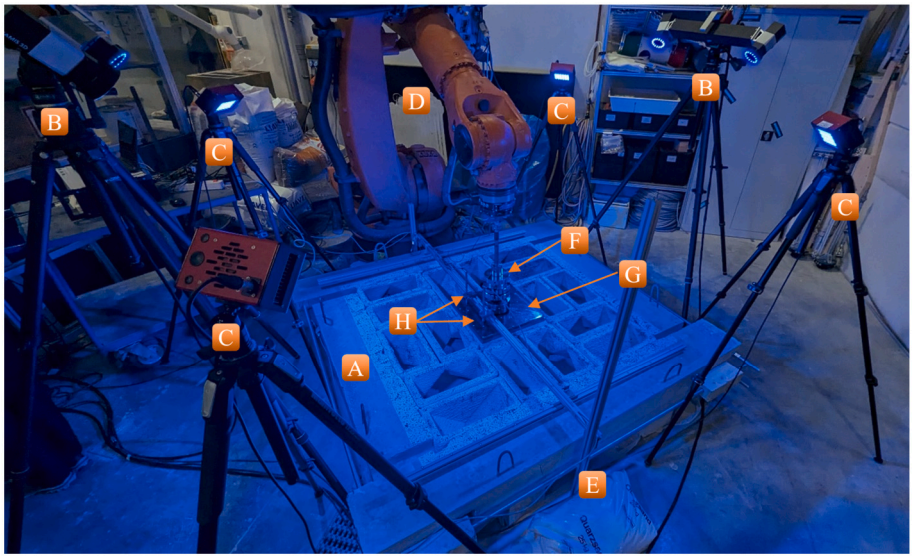

Fig. 16. Test setup for testing the composite ceiling (A) with ARAMIS 3D 12M sensor (B), exposure (C), industrial robot (D), reference frame (E), load cell (F), load application plate (G) and LVDTs (H).

ensures that the load will be distributed evenly. The frame together with the topological interlocking blocks was then lifted with an indoor crane and the frame was placed on concrete cubes with an edge length of 20 cm, which serve as bearing points, see Fig. 15b. By lifting up the frame the load-bearing behaviour of the TIA was activated. A 5 cm high layer of perlite fill material, the same as for printing, was spread out on the floor under the blocks to protect the floor from damage in the event of failure.

The entire composite ceiling was grounded with white paint. By adding random black speckles, a unique spray pattern was created, as required for the digital image correlation. A reference frame was also produced for the photogrammetry. The frame, made of aluminium profiles, is decoupled from the composite ceiling and the load arm and is intended to act as a reference coordinate system to absorb possible deformation of the composite ceiling. Two LVDTs (Linear Variable Differential Transformator) with a measurement range of 50 mm were attached to this reference frame to measure the movement of the load transfer plate. The two-part plate made of plastic and iron covered the two centre topological interlocking blocks measuring 40 x 40 cm^2. The lower part of the load introduction plate was made of plastic. The soft plastic is designed to absorb unevenness from the blocks and was levelled on the blocks with gypsum. The upper part made of steel ensures a planar load introduction.

The industrial robot described in Section 5.3 was used to apply the load onto the two central blocks, as seen previously in the numerical simulation in Section 4. The load was applied distance-controlled with a speed of 2.5 mm/s. A load cell U9B Hottinger Brüel and Kjaer GmbH with a load capacity of 50 kN and a spherical cap were screwed to the adapter flange of the robot, which was later used to press on the load transfer plate. Reference points for digital image correlation (DIC) were glued to the frame of the composite ceiling, the load application plate, the load cell and the reference frame. This made it possible to track the relative individual movements of all parts.

An opulent photogrammetry system was provided by the company Carl Zeiss GOM Metrology GmbH and set up and commissioned by an employee. Two ARAMIS 3D 12M systems were used to capture the entire surface of the composite ceiling, see Fig. 16. The measurements were carried out from two sides in order to avoid any gaps due to concealment of reference frames or load arms. In addition, four exposure systems were used to ensure uniform illumination. All measurements, including

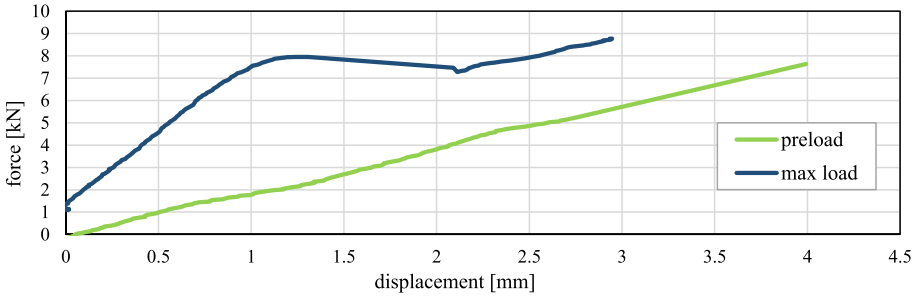

Fig. 17. Force-displacement curve from pre-loading and loading.

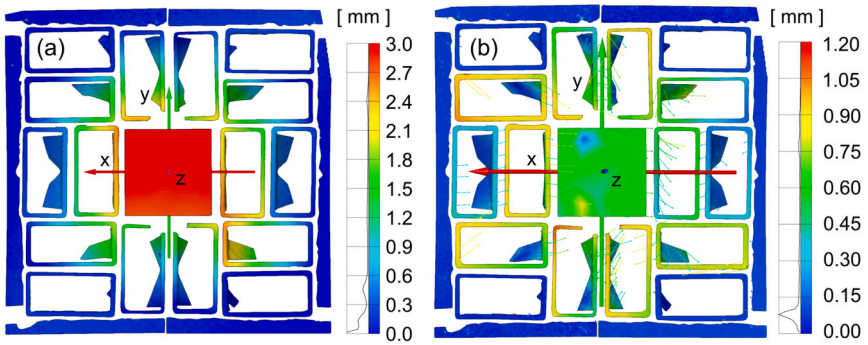

Fig. 18. Deformation during the second test at maximum load of 8.76 kN (a) in the z-direction and (b) in the $x-y$-direction.

those from the LVDT and load cell, were bundled in a measurement programme in the Gom software.

6.2. Testing and results

The composite ceiling test is a bending test of a slab supported on all sides with a point load applied in the centre. The frame generates an external preload on the topological interlocking blocks and ensures that they are restrained, as the geometry significantly prevents the blocks from twisting. The load is applied in a distance-controlled manner using a robot arm, to which a spherical cap and a load cell are attached. For load application, these were positioned vertically and centrally above the load application plate using photogrammetric measurement. The photogrammetric image acquisition was then started in the GOM Correlate Pro software and the industrial robot was moved vertically downwards. The test ended either when the composite ceiling failed or with an emergency shutdown of the robot to protect it from damage. At the end of the test, the image acquisition was recorded, stopped and saved in the GOM software.

During the test, the deflection and deformation were recorded as functions of the load for all blocks in the assembly, the composite ceiling, and the load frame. Predicting the expected breaking load manually was not feasible due to the complexity of the composite ceiling. It was hypothesised that the unreinforced topological interlocking blocks would not bear large loads, close to the tensile strength of the concrete, and that these loads would be further reduced by potential imperfections resulting from the 3D printing process and interlocking effects. The testing setup with the robot arm was selected as the initial test method because it could be realised with minimal time and financial resources.

Contrary to expectations, the slab-system could not be destroyed by the load applied by the robot arm. The first load was applied over 35 seconds, during which the force increased linearly and reached a maximum of 7.63 kN at a deflection of 3.9 mm, until the robot's emergency stop was activated. The robot's limit value was reached, and the test concluded before the blocks failed.

On the one hand, it was surprising that the composite ceiling could withstand this load, but on the other hand, it was disappointing that the ceiling was not brought to the end of its load-bearing capacity. Consequently, an attempt was made to increase the load. During the second load test, two heavy iron plates were placed on the middle of two topological interlocking blocks, creating a dead load of 1.11 kN. After placing the iron plates in the middle of the ceiling, the deflection was zeroed. During the test, the increase in force was significantly higher than in the first test, which indicates a higher stiffness. After 15 seconds, the force dropped from 7.95 kN to 7.45 kN, causing the topological interlocking blocks to slide together, which resulted in the deflection jumping from 1.23 mm to 2.11 mm. The force then continued to increase linearly, but at a flatter angle, until the robot's limit value was reached. With the second load, a maximum load of 8.76 kN was achieved with a deflection of 2.95 mm. The end of the test was triggered again by the robot's emergency shutdown. Cracks in the blocks were not detected at any point during the load application. The force-displacement curve from the first and second loading is shown in the diagram in Fig. 17. The deformation after the load was removed was approximately 1 mm.

The deformation analysis at the point of maximum load of the second test, namely 8.76 kN, using the photogrammetric measurement system is illustrated in colour in Fig. 18. The displacement was analysed both in the load direction (z-direction) and in the $x-y$ plane. Fig. 18 (a) shows the displacement in the z-direction, whereby the movement of the load introduction plate is clearly recognisable. The deformation of the composite ceiling is most pronounced here and decreases from the centre to the edges. No deformation was detected on the load frame. The deformation shows an approximate symmetry, with only the lower right corner of the load introduction plate and the neighbouring blocks showing increased deformation. The deformation in the $x-y$-direction is less pronounced than in the z-direction, which is why a different scale was selected for better visualisation, see Fig. 18 (b). On the left side, the displacement is more pronounced and reaches a maximum of 1.1 mm. Two artefacts caused by the LVDTs became visible in the measurement on the load introduction plate.

Through an in-depth analysis of the results, a deflection was extracted in both the x- and y-directions, as shown in Fig. 19. Points were set from the centre point to the edge of the component in order to record the maximum deformation both at the time of the highest load

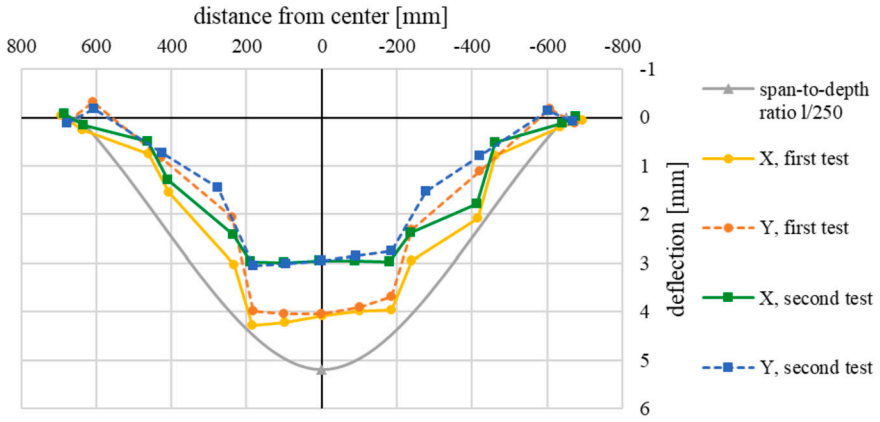

Fig. 19. Measured deflection of the composite ceiling in *x*- and *y*-direction under maximum of the first and second test in comparison with the span-to-depth ratio 1/250.

Fig. 20. (a) Demounted parts of the ceiling. (b) The 18 blocks used in the experiments were reused together with other blocks to build a large-scale demonstrator composed of 54 blocks.

from the first and the second test. The coordinate system introduced in Fig. 18 was used. DIN 1045-1:2023-08 [28], a standard for design of structures made of concrete, reinforced concrete or prestressed concrete, was used to evaluate the measured deflection in relation to the span-to-depth ratio. This standard specifies that in the serviceability limit state, the maximum deflection in the centre of the component should not be greater than 1/250 of the length of the component. For a length of 1300 mm, this means a maximum deflection of 5.2 mm. These limit values were also entered in grey in the diagram in order to be able to make an assessment (see Fig. 19). The analysis shows that the bending lines of the composite floor as a whole were within the prescribed maximum deflection limits and were therefore within the serviceability limit state. Furthermore, a slight misalignment of the load introduction plate can be recognised in the measured bending lines, but this is only a few tenths of a millimetre. The asymmetry of the bending lines in the *x*- and *y*-directions is due to the load-bearing behaviour of the topological interlocking blocks. As the load is initially transferred in the *x*-direction, the deformations in this direction are also greater than in the *y*-direction.

Following the completion of the test, the composite ceiling was dismantled (Fig. 20a). No cracks or spalling were found on the blocks or the load frame. The topological interlocking blocks were mounted in a different construction and successfully reused, see Fig. 20b.

7. Conclusion and outlook

This work demonstrates that the concept of topological interlocking assemblies and related challenges are compatible with the manufacturing method of 3D concrete printing. The main challenge of creating a continuous and efficient printing path led us to consider blocks based on the methods outlined in [13]. Their design allows the surfaces to be triangulated and easily divided into layers of fundamental domains, making them particularly well-suited for 3D concrete printing. While other block designs can also be realised using 3D-printing techniques, this feature provides a distinct advantage for the manufacturing approach. To maintain high and consistent print quality, which is crucial for the success of interlocking in the assembly, we proposed a filament path generation method that ensures continuous and uniform nozzle movement. Three different geometries were printed to assess this method: the Versatile Block, the RhomBlock, and the 3-Diamond Block. The selected assembly of 18 Versatile Blocks was initially analysed by simulating its mechanical behaviour. The numerical results showed good agreement with experimental data, validating the simulation approach. This validated model will be used in future studies to optimise the structure and further develop such 3D-printed assemblies Furthermore, the Versatile Blocks, which were selected for further investigation, were produced in small quantities and assembled into a composite slab. The initial tests demonstrated the interlocking effect and a clear load transfer of the topological interlocking to the frame. The results of the mechanical performance of this construction exceeded all expectations. When a load is applied to the composite ceiling, the gap between the blocks permits relative motion, enabling the structure to reconfigure itself until an equilibrium is achieved. Therefore the structure has to be preloaded to minimise settlement and vibration of the blocks during assembly may be considered. Preloading TIA for both experimental and numerical experiments has also been previously documented in other works, see for instance [9,23,34]. It was demonstrated that the TIA of choice displayed

a relatively small deflection in the order of the size of the assembly, i.e. the investigation of the composite ceiling with a span of 1.3 x 1.3 m^2 could support a load of 8.8 kN, with a maximum load-induced deflection of 3 mm in the given test environment. In civil engineering, such modular assemblies could be utilised, for instance, as lightweight ceiling structures. Since the blocks are not permanently connected, they can be easily disassembled and reused, representing a significant step toward sustainable construction practices.

In summary, this study underscores the potential of 3D concrete printed topological interlocking blocks for innovative and sustainable construction solutions. The positive outcomes suggest further exploration into optimising and expanding the applications of these versatile blocks in various construction scenarios. Significant advancements in this field are anticipated, driven by the promising results obtained.

CRediT authorship contribution statement

Tom Goertzen: Writing – review & editing, Writing – original draft, Visualization, Software, Methodology, Investigation, Formal analysis, Conceptualization. **Tobias Neef:** Writing – review & editing, Writing – original draft, Validation, Resources, Methodology, Investigation, Formal analysis, Conceptualization. **Philipp Scheffler:** Validation, Software, Investigation, Formal analysis, Conceptualization. **Domen Macek:** Writing – review & editing, Writing – original draft, Visualization, Validation, Software, Methodology, Formal analysis, Conceptualization. **Viktor Mechtcherine:** Writing – review & editing, Supervision, Funding acquisition, Conceptualization. **Alice C. Niemeyer:** Writing – review & editing, Supervision, Funding acquisition, Conceptualization.

Funding

This work was funded by the Deutsche Forschungsgemeinschaft (DFG, German Research Foundation) – SFB/TRR 280. Project-ID: 417002380. Additionally, Tom Goertzen acknowledges financial support from the Australian Government through the Australian Research Council's Discovery Projects funding scheme (project DP230102982).

Declaration of competing interest

The authors declare that they have no known competing financial interests or personal relationships that could have appeared to influence the work reported in this paper.

Data availability

Data will be made available on request.

References

[1] Reymond Akpanya, Tom Goertzen, Sebastian Wiesenhuetter, Alice C. Niemeyer, Jörg Noennig, Topological interlocking, Truchet tiles and self-assemblies. A construction-kit for civil engineering design, in: Judy Holdener, Eve Torrence, Chamberlain Fong, Katherine Seaton (Eds.), Proceedings of Bridges 2023: Mathematics, Art, Music, Architecture, Culture, Tessellations Publishing, Phoenix, Arizona, 2023, pp. 61–68.

[2] Ergun Akleman, Vinayak R. Krishnamurthy, Chia-An Fu, Sai Ganesh Subramanian, Matthew Ebert, Matthew Eng, Courtney Starrett, Haard Panchal, Generalized abeille tiles: topologically interlocked space-filling shapes generated based on fabric symmetries, Comput. Graph. 89 (2020) 156–166.

[3] Mois I. Aroyo (Ed.), International Tables for Crystallography, Volume A: Space-Group Symmetry, Volume A, 6th edition, Wiley, December 2016.

[4] Zeeshan Ahmed, Rob Wolfs, Freek Bos, Theo Salet, A framework for large-scale structural applications of 3D printed concrete: the case of a 29 m bridge in the Netherlands, Open Conf. Proc. 1 (feb 2022) 5–19.

[5] A.V. Dyskin, Y. Estrin, A.J. Kanel-Belov, E. Pasternak, A new concept in design of materials and structures: assemblies of interlocked tetrahedron-shaped elements, Scr. Mater. 44 (12) (2001) 2689–2694.

[6] A.V. Dyskin, Y. Estrin, E. Pasternak, H.C. Khor, A.J. Kanel-Belov, Fracture resistant structures based on topological interlocking with non-planar contacts, Adv. Eng. Mater. 5 (3) (March 2003) 116–119.

[7] A.V. Dyskin, Yuri Estrin, E. Pasternak, Topological interlocking materials, in: Yuri Estrin, Yves Bréchet, John Dunlop, Peter Fratzl (Eds.), Architectured Materials in Nature and Engineering: Archimats, Springer International Publishing, Cham, 2019, pp. 23–49.

[8] Lee Vasilios Djumas, Design, Fabrication and Characterisation of Topological Interlocking Structures Utilising Additive Manufacturing, Phd thesis, Monash University, 2018.

[9] Lee Djumas, George P. Simon, Yuri Estrin, Andrey Molotnikov, Deformation mechanics of non-planar topologically interlocked assemblies with structural hierarchy and varying geometry, Sci. Rep. 7 (1) (September 2017) 11844.

[10] Y. Estrin, A.V. Dyskin, E. Pasternak, Topological interlocking as a material design concept, Mater. Sci. Eng. C 31 (6) (2011) 1189–1194.

[11] Yuri Estrin, Vinayak R. Krishnamurthy, Ergun Akleman, Design of architectured materials based on topological and geometrical interlocking, J. Mater. Res. Technol. 15 (2021) 1165–1178.

[12] Tom Goertzen, Domen Macek, Lukas Schnelle, Meike Weiß, Stefanie Reese, Hagen Holthusen, Alice C. Niemeyer, Influence of block arrangement on mechanical performance in topological interlocking assemblies. A study of the versatile block, Int. J. Solids Struct. 306 (2025) 113102.

[13] Tom Goertzen, Alice Niemeyer, Wilhelm Plesken, Topological Interlocking via Symmetry, Proc. of the 6th fib International Congress 2022, vol. 06, Novus Press, Oslo, Norway, 2022.

[14] Tom Goertzen, Constructing interlocking assemblies with crystallographic symmetries, arXiv e-prints, arXiv:2405.15080, May 2024.

[15] Tom Goertzen, Mathematical foundations of interlocking assemblies, arXiv e-prints, arXiv:2405.17644, May 2024.

[16] Kevin Harsono, Shen-Guan Shih, Felicia Wagiri, William Alfred, Integration of design and performance evaluation for reusable osteomorphic-block masonry, Nexus Netw. J. (October 2023).

[17] Egor Ivaniuk, Martin Friedrich Eichenauer, Zlata Tošić, Steffen Müller, Daniel Lordick, Viktor Mechtcherine, 3d printing and assembling of frame modules using printable strain-hardening cement-based composites (shcc), Mater. Des. 219 (2022) 110757.

[18] A. Rezaee Javan, H. Seifi, S. Xu, D. Ruan, Y.M. Xie, The impact behaviour of plate-like assemblies made of new interlocking bricks: an experimental study, Mater. Des. 134 (2017) 361–373.

[19] A. Rezaee Javan, H. Seifi, S. Xu, X. Lin, Y.M. Xie, Impact behaviour of plate-like assemblies made of new and existing interlocking bricks: a comparative study, Int. J. Impact Eng. 116 (2018) 79–93.

[20] Anooshe Rezaee Javan, Hamed Seifi, Shanqing Xu, Yi Min Xie, Design of a new type of interlocking brick and evaluation of its dynamic performance, in: Proceedings of IASS Annual Symposia, IASS 2016 Tokyo Symposium: Spatial Structures in the 21st Century – New Approaches, Materials & Construction Methods, Tokyo, Japan, International Association for Shell and Spatial Structures (IASS), September 2016, pp. 1–8, Backup Publisher: International Association for Shell and Spatial Structures (IASS) Type: Research Article.

[21] A.J. Kanel-Belov, A.V. Dyskin, Y. Estrin, E. Pasternak, I.A. Ivanov-Pogodaev, Interlocking of convex polyhedra: towards a geometrical theory of fragmented solids, Mosc. Math. J. 10 (2) (2010) 337–342.

[22] S. Khandelwal, T. Siegmund, R.J. Cipra, J.S. Bolton, Transverse loading of cellular topologically interlocked materials, Int. J. Solids Struct. 49 (18) (2012) 2394–2403.

[23] S. Khandelwal, T. Siegmund, R.J. Cipra, J.S. Bolton, Adaptive mechanical properties of topologically interlocking material systems, Smart Mater. Struct. 24 (4) (March 2015) 045037.

[24] Steven Laudage, Ethan Guenther, Thomas Siegmund, Design and analysis of a lightweight beam-type topologically interlocked material system, Structures 51 (2023) 1402–1413.

[25] Francesca Lecci, Cecilia Mazzoli, Cristiana Bartolomei, Riccardo Gulli, Design of flat vaults with topological interlocking solids, Nexus Netw. J. 23 (3) (September 2021) 607–627.

[26] Yu Li, Hao Wu, Xinjie Xie, Liming Zhang, Philip F. Yuan, Yi Min Xie, FloatArch: a cable-supported, unreinforced, and re-assemblable 3D-printed concrete structure designed using multi-material topology optimization, Addit. Manuf. 81 (February 2024) 104012.

[27] A. Molotnikov, Y. Estrin, A.V. Dyskin, E. Pasternak, A.J. Kanel-Belov, Percolation mechanism of failure of a planar assembly of interlocked osteomorphic elements, Eng. Fract. Mech. 74 (8) (2007) 1222–1232.

[28] DIN-Normenausschuss Bauwesen (NABau), DIN Standards Committee Building, Civil Energeering, DIN Deutsches Institut für Normung e. V., and DIN German Institute for Standardization, DIN 1045-1 Tragwerke aus Beton, Stahlbeton und Spannbeton - Teil 1: Planung, Bemessung und Konstruktion, 2023-08-00.

[29] Tobias Neef, Marko Butler, Viktor Mechtcherine, Integrating mineral-bonded carbon fibers into 3D concrete printing, in: Proceedings for the 6th fib International Congress 2022, Oslo, 2022, pp. 604–613.

[30] Tobias Neef, Gözdem Dittel, Martin Scheurer, Thomas Gries, Viktor Mechtcherine, Utilizing textiles as integrated formwork for additive manufacturing with concrete, in: Alper Ilki, Derya Çavunt, Yavuz Selim Çavunt (Eds.), Building for the Future: Durable, Sustainable, Resilient, Springer Nature Switzerland, Cham, 2023, pp. 1285–1292.

[31] M. Rippmann, T. Van Mele, M. Popescu, E. Augustynowicz, T. Méndez Echenagucia, C. Calvo Barentin, U. Frick, P. Block, The Armadillo Vault: computational design and

digital fabrication of a freeform stone shell, in: Advances in Architectural Geometry 2016, September 2016, pp. 344–363.
[32] Thomas Siegmund, Francois Barthelat, Raymond Cipra, Ed Habtour, Jaret Riddick, Manufacture and mechanics of topologically interlocked material assemblies, Appl. Mech. Rev. 68 (040803) (July 2016).
[33] Kai Schneider, Marko Butler, Viktor Mechtcherine, Carbon Concrete Composites C3 – Nachhaltige Bindemittel und Betone für die Zukunft, Beton- Stahlbetonbau 112 (12) (2017) 784–794.
[34] S. Schaare, A.V. Dyskin, Y. Estrin, S. Arndt, E. Pasternak, A. Kanel-Belov, Point loading of assemblies of interlocked cube-shaped elements, Int. J. Eng. Sci. 46 (12) (2008) 1228–1238.
[35] Sai Ganesh Subramanian, Mathew Eng, Vinayak R. Krishnamurthy, Ergun Akleman, Delaunay Lofts: a biologically inspired approach for modeling space filling modular structures, Comput. Graph. 82 (2019) 73–83.
[36] M. Short, T. Siegmund, Scaling, growth, and size effects on the mechanical behavior of a topologically interlocking material based on tetrahedra elements, J. Appl. Mech. 86 (11) (09 2019) 111007.
[37] Oliver Tessmann, Andrea Rossi, Geometry as interface: parametric and combinatorial topological interlocking assemblies, J. Appl. Mech. 86 (September 2019) 111002.
[38] Gieljan Vantyghem, Wouter De Corte, Emad Shakour, Oded Amir, 3d printing of a post-tensioned concrete girder designed by topology optimization, Autom. Constr. 112 (2020) 103084.
[39] Vera Viana, From solid to plane tessellations, and back, Nexus Netw. J. 20 (3) (December 2018) 741–768.
[40] Yuxin Wang, Farhad Aslani, Arcady Dyskin, Elena Pasternak, Digital twin applications in 3D concrete printing, Sustainability 15 (3) (2023).
[41] Michael Weizmann, Oded Amir, Yasha Jacob Grobman, Topological interlocking in buildings: a case for the design and construction of floors, Autom. Constr. 72 (2016) 18–25.
[42] Michael Weizmann, Oded Amir, Yasha Jacob Grobman, Topological interlocking in architecture: a new design method and computational tool for designing building floors, Int. J. Archit. Comput. 15 (2) (2017) 107–118, https://doi.org/10.1177/1478077117714913.
[43] Li Wang, Yi Liu, Yu Yang, Yanfeng Li, Mingke Bai, Bonding performance of 3D printing concrete with self-locking interfaces exposed to compression–shear and compression–splitting stresses, Addit. Manuf. 42 (2021) 101992.
[44] Ziqi Wang, Peng Song, Florin Isvoranu, Mark Pauly, Design and structural optimization of topological interlocking assemblies, ACM Trans. Graph. 38 (6) (November 2019).
[45] Wenzheng Xu, Xiaoshan Lin, Pengda Li, Yu-Fei Wu, Yi Min Xie, Impact behaviour of tunnel lining assembled from non-planar interlocking steel fibre reinforced concrete bricks, Eng. Struct. 296 (December 2023) 116907.
[46] Wenzheng Xu, Xiaoshan Lin, Yi Min Xie, A novel non-planar interlocking element for tubular structures, Tunn. Undergr. Space Technol. 103 (September 2020) 103503.
[47] Hsien Ta, David Yong, Utilisation of Topologically-Interlocking Osteomorphic Blocks for Multi-Purpose Civil Construction, Phd thesis, University of Western Australia, 2011.
[48] Babak Zareiyan, Behrokh Khoshnevis, Effects of interlocking on interlayer adhesion and strength of structures in 3d printing of concrete, Autom. Constr. 83 (2017) 212–221.